JOURNAL OF MATERIALS SCIENCE **34** (1999) 3721–3729

Preparation, characterization and photoelectrochemical behaviors of Fe(III)-doped TiO_2 nanoparticles

YANQIN WANG, HUMIN CHENG*, YANZHONG HAO, JIMING MA, WEIHUA LI, SHENGMIN CAI
Department of Chemistry, Peking University, Beijing, 100871, People's Republic of China
E-mail: majm@chemms.chem.pku.edu.cu

Fe(III)-doped TiO_2 nanoparticles with different Fe(III) content (at %, nominal) have been prepared at different pH using hydrothermal method. The products were characterized by X-ray powder diffraction, transmission electron microscope, electron diffraction, diffuse reflectance spectra, XPS and spot EDX analysis. All the studies showed that anatase, brookite and trace of hematite coexisted at lower pH (1.8 and 3.6) when Fe(III) content was as low as 0.5% and the distribution of iron ions was non-uniform between particles. But at higher pH (6.0), the uniform solid solution of iron-titanium oxide formed. The photoelectrochemical properties were studied by measuring photocurrent at different electrode potentials and the results showed the phenomena of p-n photoresponse existence in samples prepared at pH 1.8–6.0. © *1999 Kluwer Academic Publishers*

1. Introduction

Solar energy conversion has been studied widely due to the depletion of the available energy sources. Titanium dioxide was used not only as photocatalyst but also as photoanode in photoelectrochemical solar cells (such as Grätzel-Type solar energy cell [1]) because of its chemical stability, low cost and non-toxicity, however titanium dioxide only absorbs near-UV light (Eg = 3.2 eV for anatase) and doesn't match the solar light very well. Fe_2O_3 has been considered to be promising for applications in solar energy conversion because it has a bandgap (Eg = 2.2 eV) smaller than that of TiO_2, but it is liable to be photocorroded and the lifetime of photogenerated minority carriers is very short [2]. Therefore, many efforts have been made to prepare transition metal ion doped TiO_2, especially Fe(III)-doped TiO_2 in order to extend the absorption threshold to visible light and to investigate their activities as photocatalyst [3–7], such as photoassisted reduction of dinitrogen to ammonia [8, 9] and photoassisted degradation of waste materials in environment treatment. In the above studies, wet impregnation [4, 5] and coprecipitation [6] methods were used and all involved in a process of calcination at high temperature (as high as 1273 K), leading to dehydration and dehydroxylation [10] and eventually resulting in less photoactivity because the hydroxyl group on the surface has a contribution on photoactivity [11].

Considerable effort has been devoted to the study of Fe(III)-doped TiO_2 particles in order to obtain structure-property relationships [12, 13]. The most photocatalytic active sample was found to be Fe(III)-doped TiO_2 particles which contained 0.2–0.5% Fe(III) and was obtained by calcination at 773 K. By increasing either or both of the iron content and the calcination temperature, a decrease in the photocatalytic activity was found [14–16] because the solubility of iron in anatase or rutile was less than 1 wt % and hematite (α-Fe_2O_3) or pseudobrookite (Fe_2TiO_5) was formed as Fe(III) content was >1 wt %. The formation of separate phase (α-Fe_2O_3 or Fe_2TiO_5) resulted in the decrease of photocatalytic activity because of the transfer of charge carriers from TiO_2 to Fe_2O_3 (or Fe_2TiO_5). However, in 1995 Tsodikov *et al.* [17] reported that solid solutions of $Fe_x(Ti)_{1-0.75x}O_{2-\delta}$ had been prepared in more wide range of Fe content ($0.01 < x < 0.14$) with sol-gel method.

Although the photocatalytic properties were studied widely for Fe(III)-doped TiO_2 particles, the photoelectrochemical property has not been reported till now. The doping of iron ions extend the absorption threshold to longer wavelength [18], so Fe(III)-doped TiO_2 nanoparticles were prepared, characterized and their photoelectrochemical behaviors were studied in our work in order to extend the photoresponse to longer wavelength and to use the solar energy efficiently. However, a different phenomenon occurred, i.e., the p-n photoresponse conversion, and the photocurrent was much smaller than that of pure TiO_2 nanocrystalline electrode.

* Author to whom all correspondence should be addressed.

2. Experimental

2.1. Preparation of Fe(III)-doped TiO_2 nanoparticles

All samples were prepared using hydrothermal method [19, 20]. 1.34 mol · dm^{-3} $TiCl_4$ aqueous solution and 0.1 mol · dm^{-3} $FeCl_3$ aqueous solution were used as stock solution. Different quantity of $TiCl_4$ solution and $FeCl_3$ solution were mixed to make the content of Fe(III) in the mixed solution to be predetermined values. 10 mol · dm^{-3} KOH was used to adjust the pH of the media. The final volume of the solution was 50 ml and the total concentration of $TiCl_4$ and $FeCl_3$ was 0.5 mol · dm^{-3}. The feedstock of 50 ml was charged into a 100 ml Teflonlined stainless steel autoclave apparatus with an electromagnetic stirrer. The reaction mixtures were heated at a certain temperature for a definite period of time, cooled to room temperature, allowed to stand for 24 h and filtered. The precipitated products were washed with acetic acid-ammonium acetate and alcohol, then dried at 80 °C. The chemical reagents used were all of analytical reagent grade.

In this paper, Fe(III) content is referred to the nominal atom content unless otherwise indicated.

2.2. Characterization of Fe(III)-doped TiO_2 nanoparticles

All samples were analyzed by X-ray diffraction (XRD) which uses a CuK_α radiation at 40 kV, 100 mA with a graphite monochromator and scans at 4° $min^{-1}(2\theta)$ with a diffractometer to determine the phase of the reaction products. A JEM-200CX transmission electron microscope (TEM) was used to observe the morphology and size of the products. The spot EDX was analyzed with H9000 transmission electron microscope with a transmissable depth of 1–2 μm. Diffuse reflectance spectra (DRS) were recorded by Shimadzu 3100 UV-Vis-NIR Recorder Spectrometer equipped with an integration sphere and $BaSO_4$ powder was used as a standard surface. The XPS spectra were also recorded with a Perkin-Elmer PH1 5600-ci spectrometer using monochromatized AlK_α radiation for the determination of the content of iron ions on the surface and in the core of Fe(III)-doped TiO_2 nanoparticles.

2.3. Preparation of the electrodes

The preparation of electrodes was reported elsewhere [1]. In this paper, the suspension of TiO_2 or Fe(III)-doped TiO_2 with the concentration of 0.1 mol · dm^{-3} was dispersed ultrasonically before use. Two drops (ca. 0.1 ml) of the suspension were applied onto a piece of transparent conducting glass (2.0 × 1.8 cm, fluorine-doped SnO_2), then the suspension was spread with a glass rod. The sample was sintered in N_2 at 480 °C for 30 min, cooled to room temperature at once. The final area of electrode was 0.5 cm^2.

2.4. Photoelectrochemical measurements

All measurements were carried out by using a standard three-electrode system equipped with a quartz window, a saturated calomel reference electrode (SCE), a work electrode and a platinum wire counter electrode. The three electrodes were placed in separated compartments, respectively. 0.1 mol · dm^{-3} SCN^- solution (pH 4.0) was used as electrolyte. A Model 173 potentiostat was used for potentiostatic control and a Type 3036 X-Y Recorder was used for the recording of photocurrent. All potentials reported were referred to SCE. The light source was an 200 W xenon lamp with a water filter of 10 mm length to minimize IR irradiation.

All the measurements of photocurrents were carried out at room temperature.

3. Results and discussion

3.1. Characterization of Fe-doped TiO_2 nanoparticles

A series of samples with different Fe(III) content were prepared at different pH of the media and characterized with various techniques.

3.1.1. X-ray diffraction

The X-ray phase analysis of the samples prepared under different conditions are given in Figs 1–3. It can be seen from Fig. 1 that two phases of anatase and brookite coexisted at pH 1.8, and no separate phase of α-Fe_2O_3 was detected until a Fe(III) content of 30% (Fig. 1h). A separate phase of α-Fe_2O_3 began to appear when Fe(III) content was 20% at pH 3.6 (Fig. 2e) but only monophase of anatase existed when Fe(III) content was $\leq$20% at pH 6.0 (Fig. 3).

It also can be seen from the three Figs that the diffraction peaks at high 2θ ($2\theta > 50°$) shifted to higher 2θ value with the increase of Fe(III) content which indicates the formation of the solid solution of iron-titanium oxides. The radii of Fe(III) ion (0.64 nm) is smaller than that of Ti(IV) (0.69 nm), so the doping of Fe(III) makes the cell parameter smaller than that of pure TiO_2. Three samples containing 5% Fe(III) and being prepared at pH 1.8, 3.6 and 6.0, respectively, were sintered at 873 K for 2 h and their phase composition did not change (shown in Fig. 4) compared with those before sintering.

3.1.2. Transmission electron microscope

Figs 5 and 6 show the TEM and electron diffraction patterns of the samples prepared at pH 1.8 and 3.6, respectively. A very interesting phenomenon was that two kinds of nanoparticles coexisted, the smaller particles were pure TiO_2 nanoparticles or the solid solution of iron-titanium oxide with a particle size of 10–15 nm, the larger particles (50–100 nm) showed a trend to aggregate and their numbers increased with the increase of Fe(III) content. Furthermore, the morphology and the particle size of the larger particles were the same as those of pure α-Fe_2O_3 nanoparticles prepared at pH 1.8 (Fig. 6c). The electron diffraction patterns show an electron diffraction ring for smaller particles and coexistence of diffraction spot and weak ring for larger particles. The measurement of the position of the diffraction spots indicates the existence of the crystal

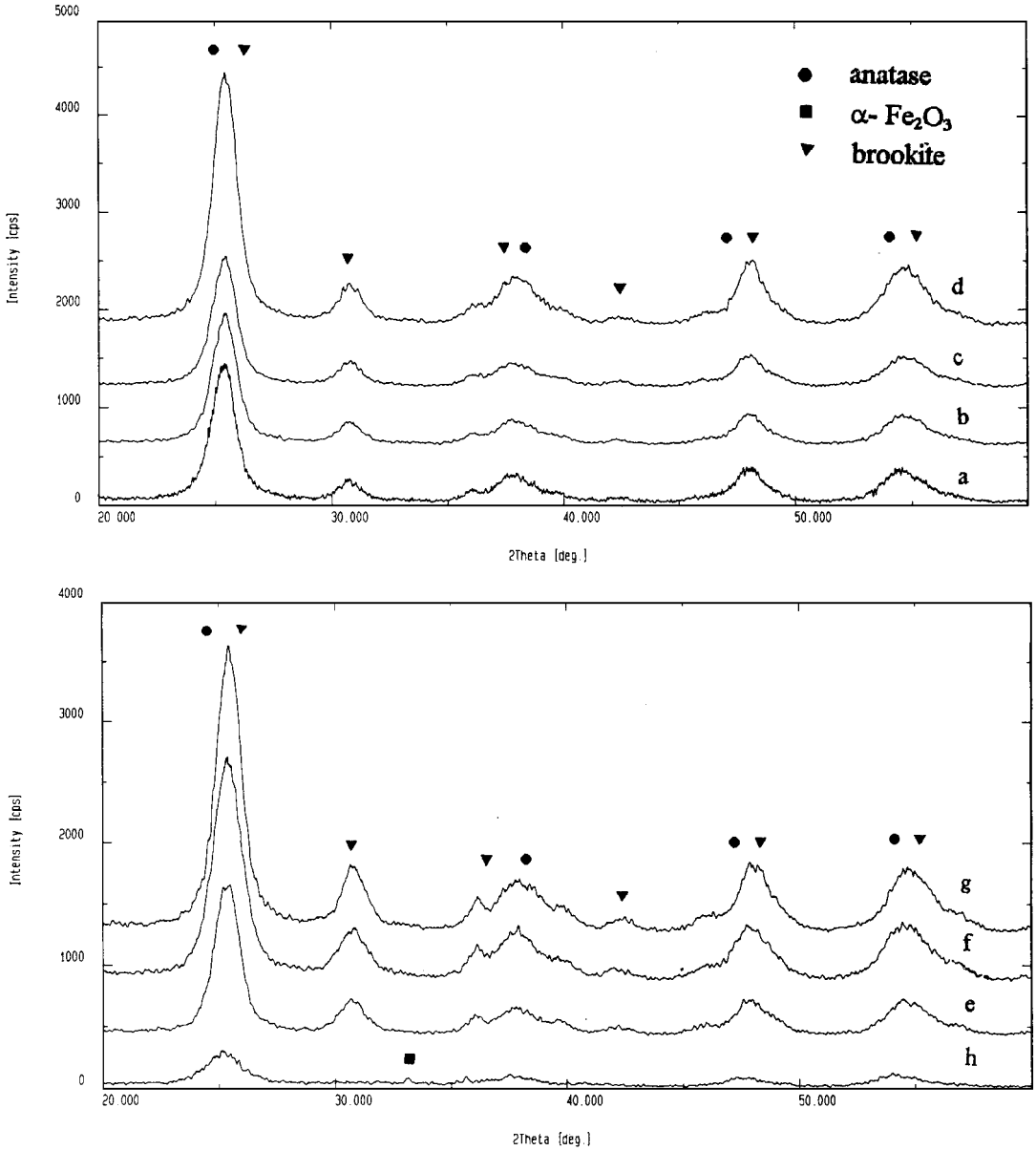

Figure 1 XRD patterns of the products at different Fe(III) content in Fe(III)-doped TiO_2 nanoparticles prepared at pH 1.8 (a) 0; (b) 0.5%; (c) 1%; (d) 2%; (e) 5%; (f) 10%; (g) 20%; and (h) 30%.

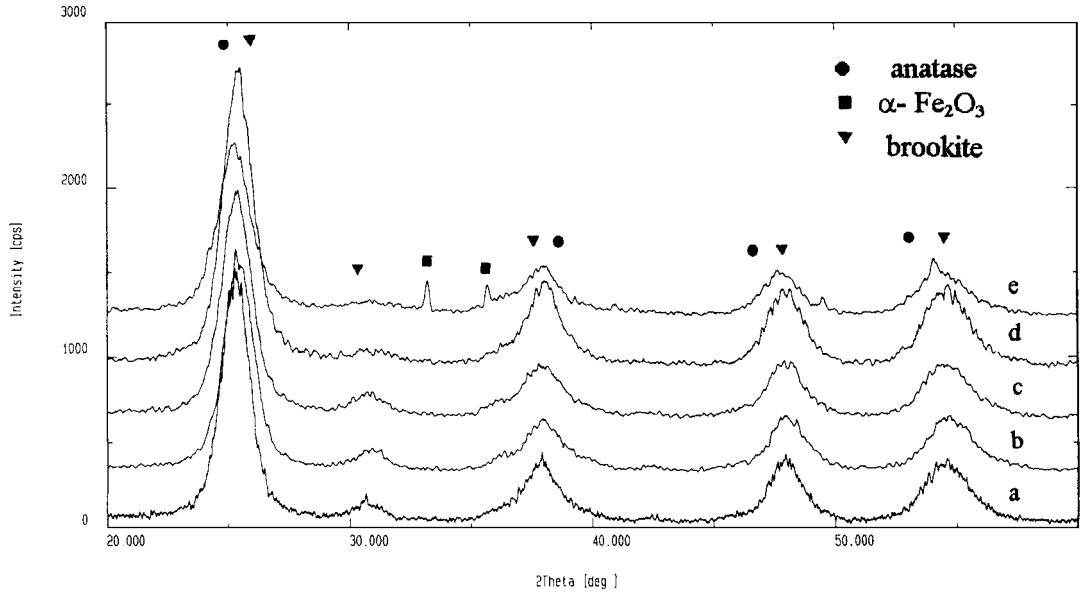

Figure 2 XRD patterns of the products at different Fe(III) content in Fe(III)-doped TiO_2 nanoparticles prepared at pH 3.6 (a) 0; (b) 2%; (c) 5%; (d) 10%; and (e) 20%.

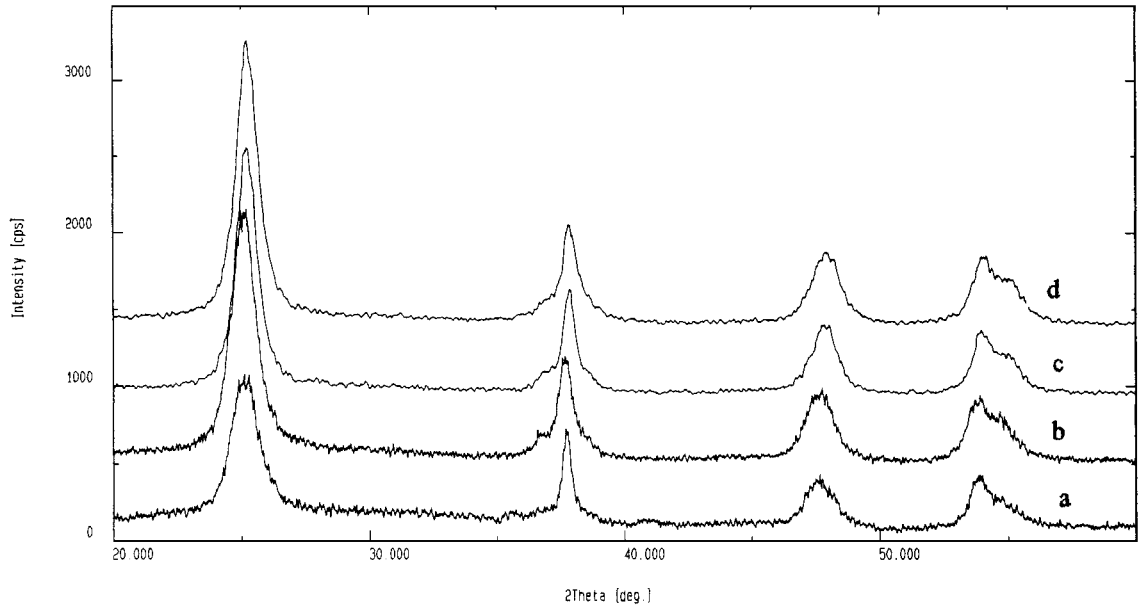

Figure 3 XRD patterns of the products at different Fe(III) content in Fe(III)-doped TiO_2 nanoparticles prepared at pH 6.0 (a) 0; (b) 2%; (c) 10%; and (d) 20%.

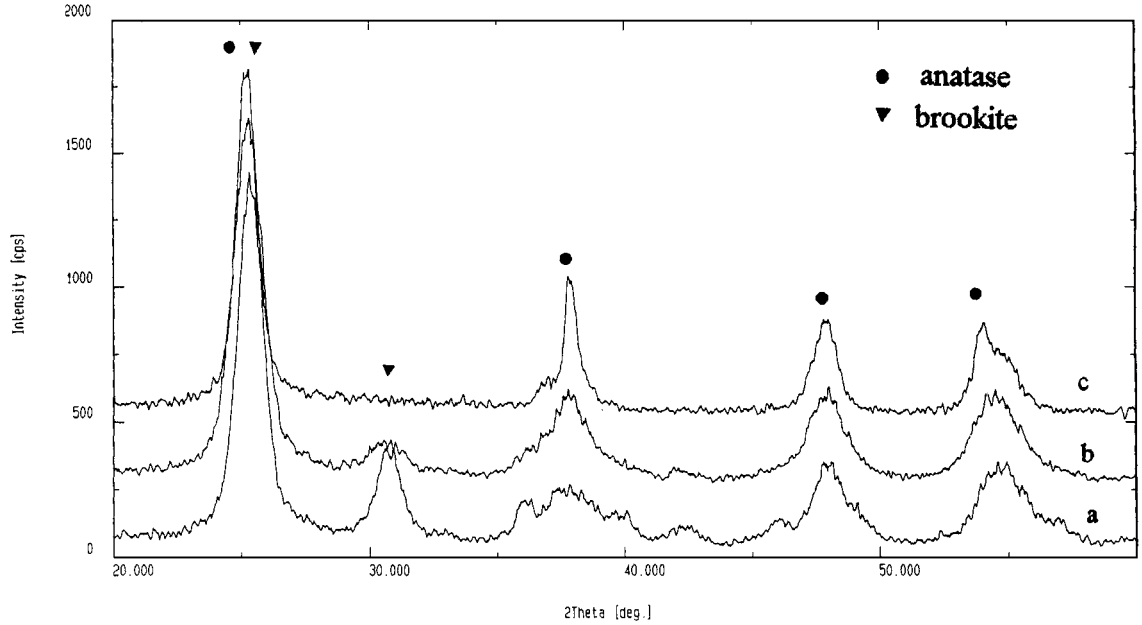

Figure 4 XRD patterns of three samples containing 5% Fe(III) sintered at 873 K for 2 h. (a) pH 1.8; (b) pH 3.6; and (c) pH 6.0.

of α-Fe_2O_3 even if it can't be detected by XRD when an nominal content of Fe(III) was as high as 10%. From the above analysis it can be proposed that the doping of Fe(III) resulted in the formation of α-Fe_2O_3 and solid solution of iron-titanoum oxides. The Fe(III)-doped TiO_2 nanoparticles prepared at pH 1.8 and 3.6 can be considered as a heterogeneous system formed by a surface solid solution and the matrix (anatase), as well as a few α-Fe_2O_3 nanoparticles.

It can be seen from Fig. 7 that no separate larger particles existed for the samples prepared at pH 6.0 and the crystals were well-formed when Fe(III) content was 2% (Fig. 7a), but it became less well-formed and amorphous when Fe(III) content was 10% (Fig. 7b). The XRD pattern shows that the cell parameters became smaller because of the doping of Fe(III) and it is possible that Fe(III) ions enter into the lattice of TiO_2 to form solid solution at pH 6.0. From the above analysis, it further confirms the difference of the structures and compositions of the samples prepared at different pH.

3.1.3. Spot EDX analysis

In the papers reported earlier [10], the distribution of iron in particles of Fe-doped TiO_2 were studied and a non-uniform distribution of iron between particles was revealed through spot EDX analysis. In this work, the similar results were obtained for samples prepared at low pH (1.8–3.6). For the sample with 10% Fe(III) prepared at pH 1.8, the result of Spot EDX showed that the content of iron reached as high as 92.1 at % in larger particles which indicated the existence of α-Fe_2O_3 while the smaller particles consisted of nearly only titanium. The result obtained from the sample with 10% Fe(III)

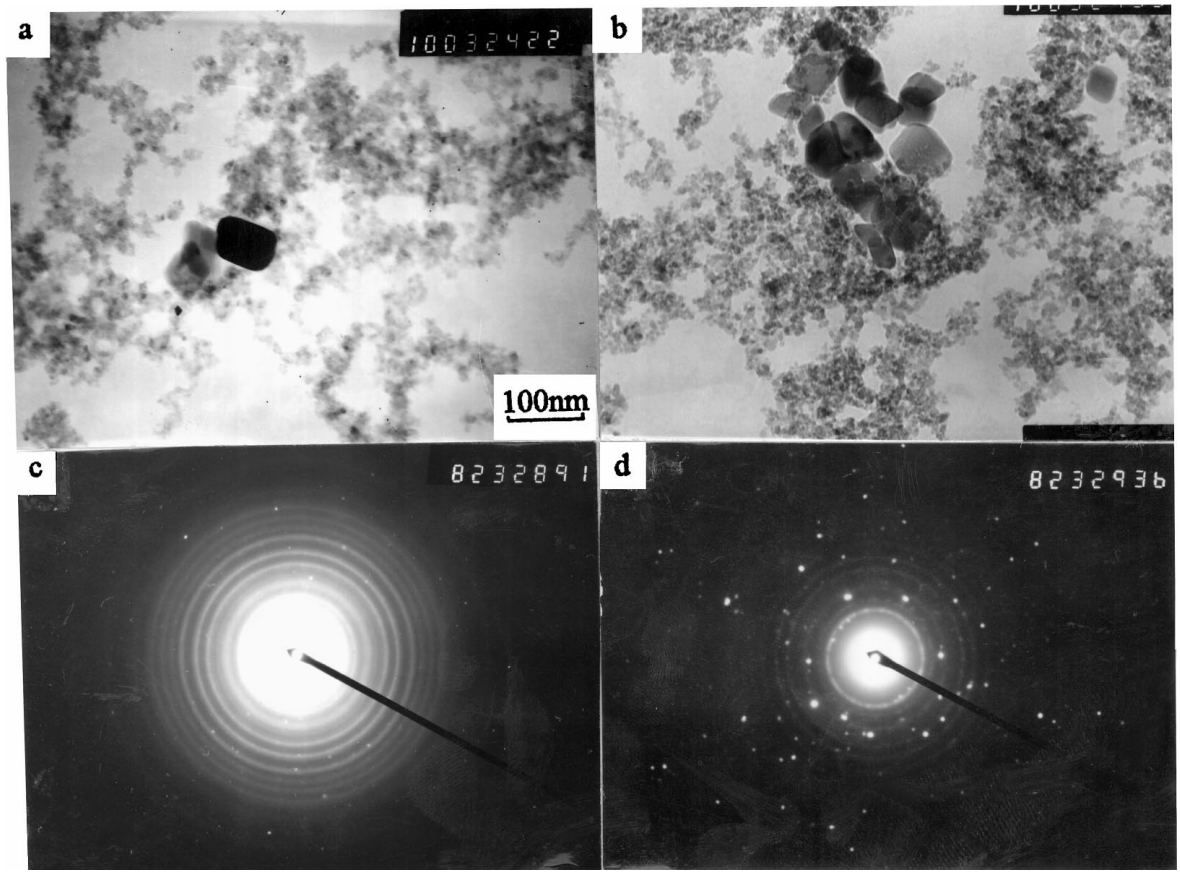

Figure 5 The TEM photographs of some selected samples at different Fe(III) content in Fe(III)-doped TiO_2 nanoparticles prepared at pH 1.8 (a) 0.5%; (b) 10%; (c) electron diffraction pattern for smaller particles in b; and (d) electron diffraction pattern for larger particles in b.

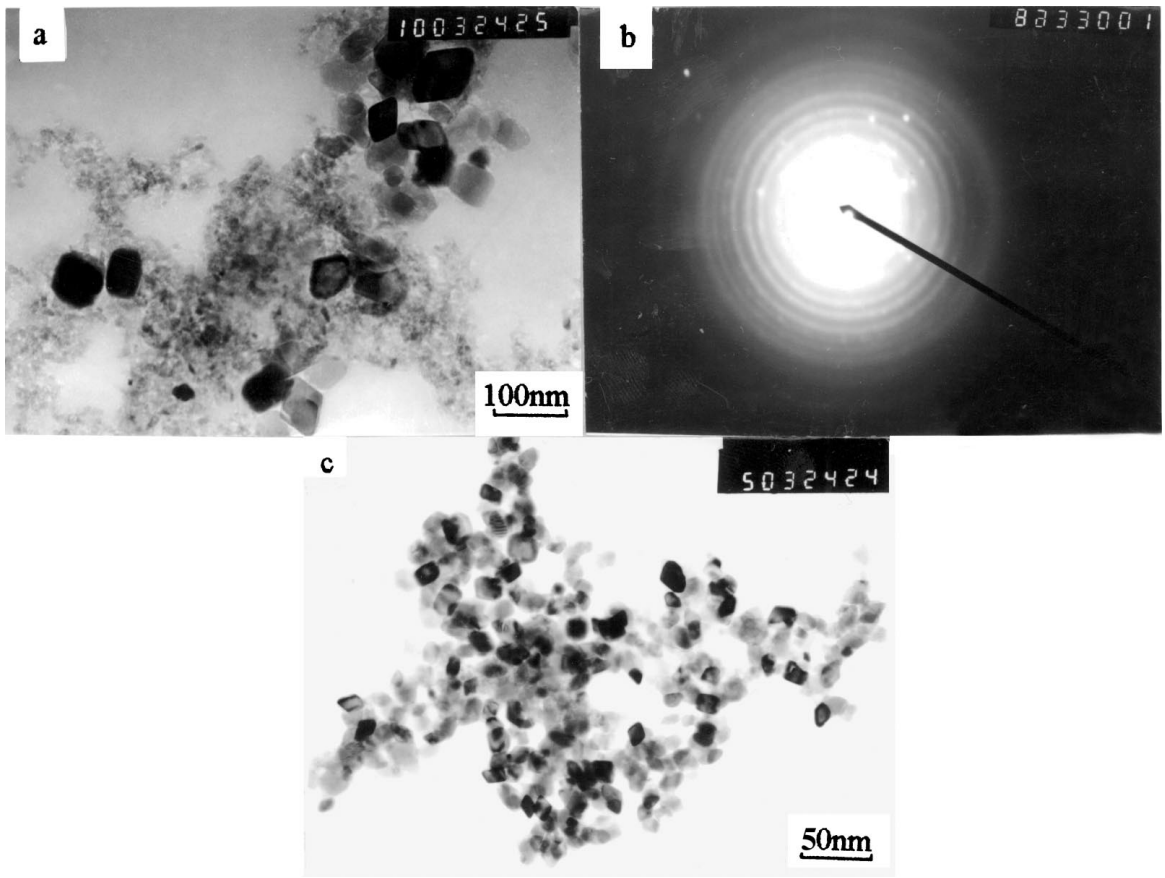

Figure 6 (a) The TEM photographs of the sample with 10% Fe(III) content in Fe(III)-doped TiO_2 nanoparticles prepared at pH 3.6; (b) electron diffraction pattern for larger particles in a; and (c) the TEM photograph of α-Fe_2O_3 prepared at pH 1.8.

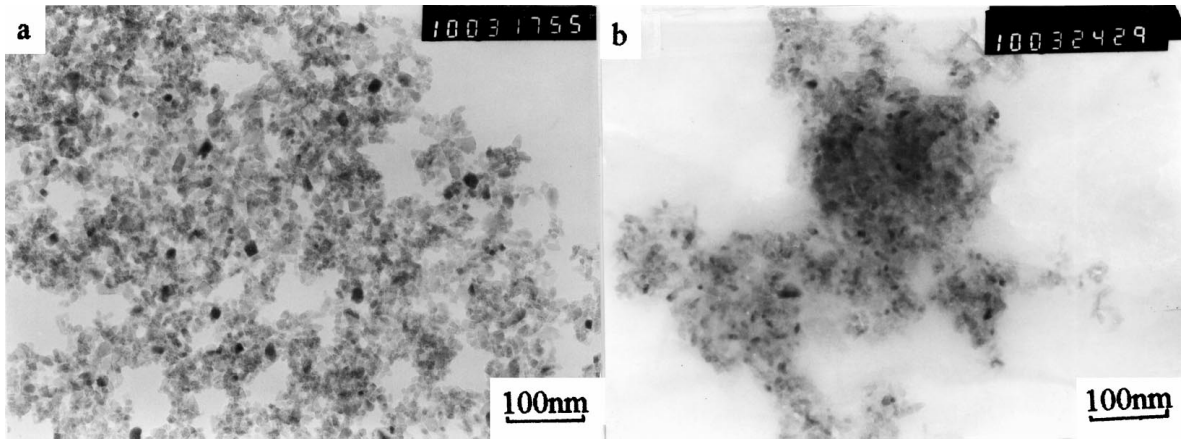

Figure 7 The TEM photographs of some selected samples at different Fe(III) content in Fe(III)-doped TiO_2 nanoparticles prepared at pH 6.0 (a) 2%; and (b) 10%.

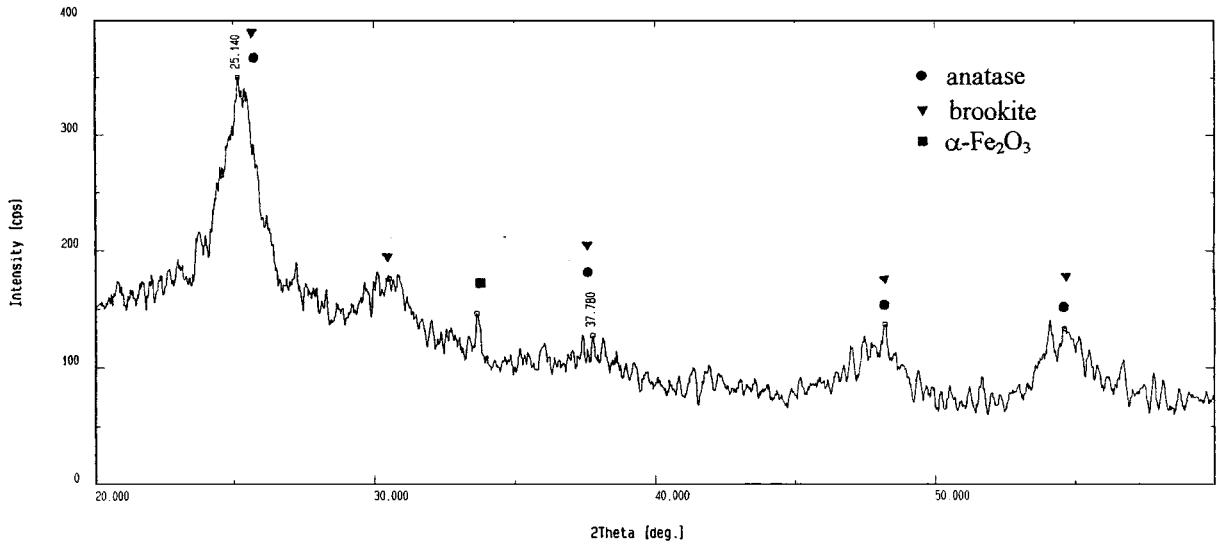

Figure 8 XRD pattern of the concentrated larger particles (pH 1.8).

prepared at pH 3.6 also showed that the iron content reached as high as 98.6 at % for larger particles (which revealed the formation of α-Fe_2O_3), but it was 12.9, 17.1 and 22.4 at %, respectively, for three different domains in small particles. For the sample with a Fe(III) content of 10% prepared at pH 6.0, the result showed that iron dispersed uniformly between particles (13.6, 12.8% respectively for two selected domains). As an additional method, the XPS pattern were also recorded for Fe(III)-doped TiO_2 nanoparticles prepared at pH 6.0 (contenting 10%, sintering at 723 K) before and after sputtering (the penetration of sputtering was 10 nm). The results showed that iron existed as Fe^{3+} in the lattice of TiO_2 and the content of Fe^{3+} before and after sputtering was the same which indicates directly that Fe^{3+} dispersed uniformly in the lattice of TiO_2 and uniform solid solution of iron-titanium oxide formed. The result was the same as that reported by Tsodikov *et al.* [17] in which the Fe(III)-doped TiO_2 nanoparticles were prepared using sol-gel method.

An additional method was used to detect the existence of α-Fe_2O_3 at lower pH, i.e., using sedimentation to collect the larger particles in the aqueous suspension of the sample contained 10% Fe(III) and prepared at pH 1.8, then determining the XRD of the collected particles. XRD shown in Fig. 8 also indicated the formation of α-Fe_2O_3 at lower pH.

3.1.4. Diffuse reflectance spectra

Fig. 9 shows the DRS of Fe(III)-doped TiO_2 nanoparticles. The absorption threshold of TiO_2 was at 390 nm (3.2 eV) and shifted to longer wavelength gradually [395 nm for 0.5%, 435 nm for 5%, 436 nm for 10% (mol) Fe(III)] with the increasing of Fe(III) content and the absorption enhanced also with increasing Fe(III) content in samples in the range of 320–500 nm, accompanying a color change from pale yellow to reddish brown. The red shift of the absorption edge of the Fe(III)-doped TiO_2 has been attributed to the excitation of 3d electrons of Fe^{3+} to the TiO_2 conduction band (charge-transfer transition) according to the energy levels proposed in reference [18].

3.1.5. Atom force microscope

Fig. 10 shows the AFM of two representative electrodes which contained 5% Fe(III) and were prepared

TABLE I The photocurrents of the samples containing 0.5% Fe(III) but prepared at different pH

pH	1.8	3.6	6.0	TiO_2
Photocurrent (μ/cm^2)	0.30	0.62	1.40	0.60

Incident light: white light.

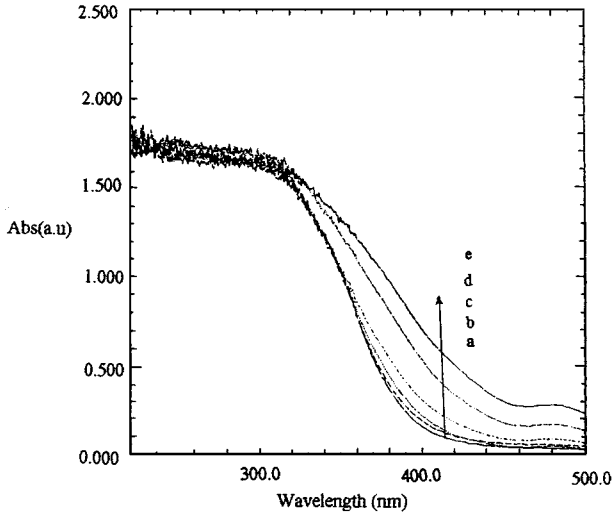

Figure 9 DRS of some samples containing different Fe(III) prepared at pH 1.8 (a) 0; (b) 0.5%; (c) 1%; (d) 2%; (e) 5%; and (f) 10%.

at pH 1.8 and 6.0, respectively. It can be seen that two kinds of particles coexisted at pH 1.8 and the smaller particles attached to larger particles, but only one kind of particles existed at pH 6.0 which were all in agreement with the results obtained from the above.

3.2. Photoelectrochemical measurements

The measurement of transient photocurrent at different electrode potentials for the samples prepared at different pH showed the similar phenomenon, i.e., the p-n photoresponse coexisted or converted. The difference is that the photoresponse increased with the increase of reaction pH for samples containing 0.5% Fe(III) and the results are shown in Table I. In order to discuss the phenomenon clearly, the following discussions are only to select the sample prepared at pH 3.6 as an example.

Fig. 11 shows the transient photocurrents of Fe(III)-doped TiO_2 nanocrystalline electrodes prepared at pH 3.6. It can be seen from Fig. 11 that the p-type photoresponse increased gradually with the increase of Fe(III) content. When Fe(III) content was 0.5%, a anodic photocurrent (n-type photoresponse) appeared only at the beginning of switching on the light, then with the prolongation of illumination time the photoresponse converted to steady cathodic photocurrent (p-type photoresponse) at the electrode potential of −0.3 V; but

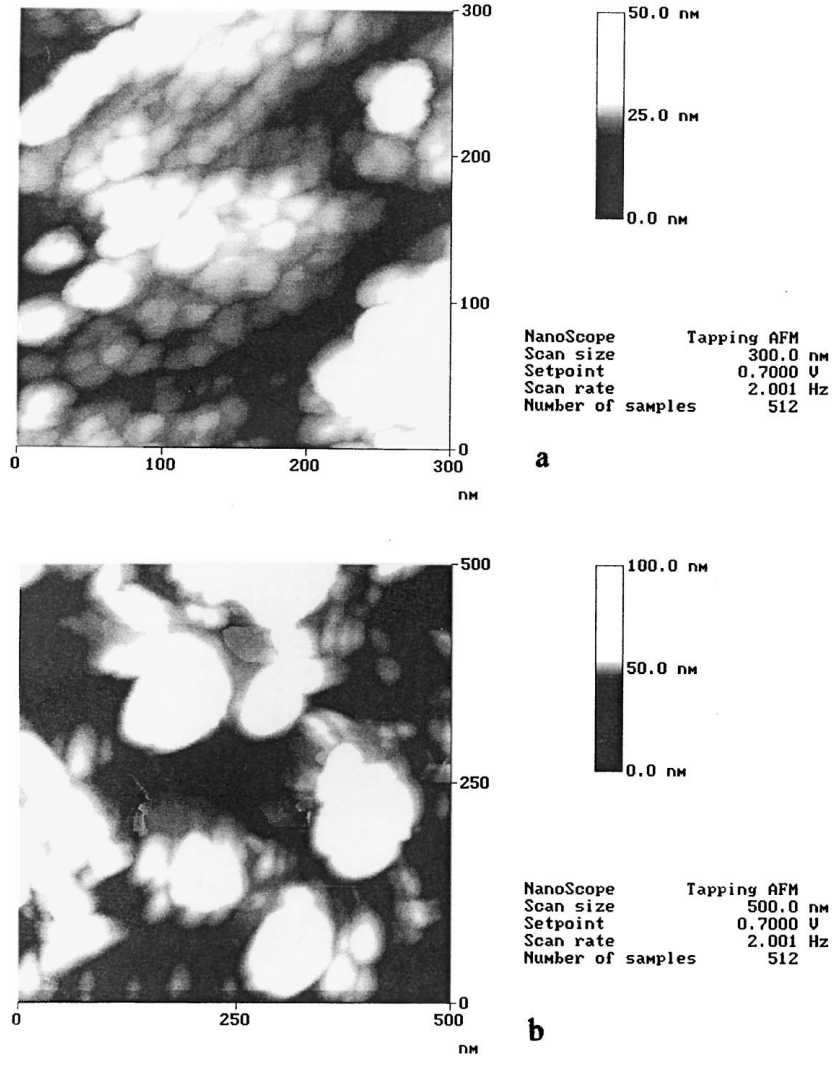

Figure 10 AFM of two electrodes (a) pH 6.0, 5% Fe(III); and (b) pH 1.8, 5% Fe(III).

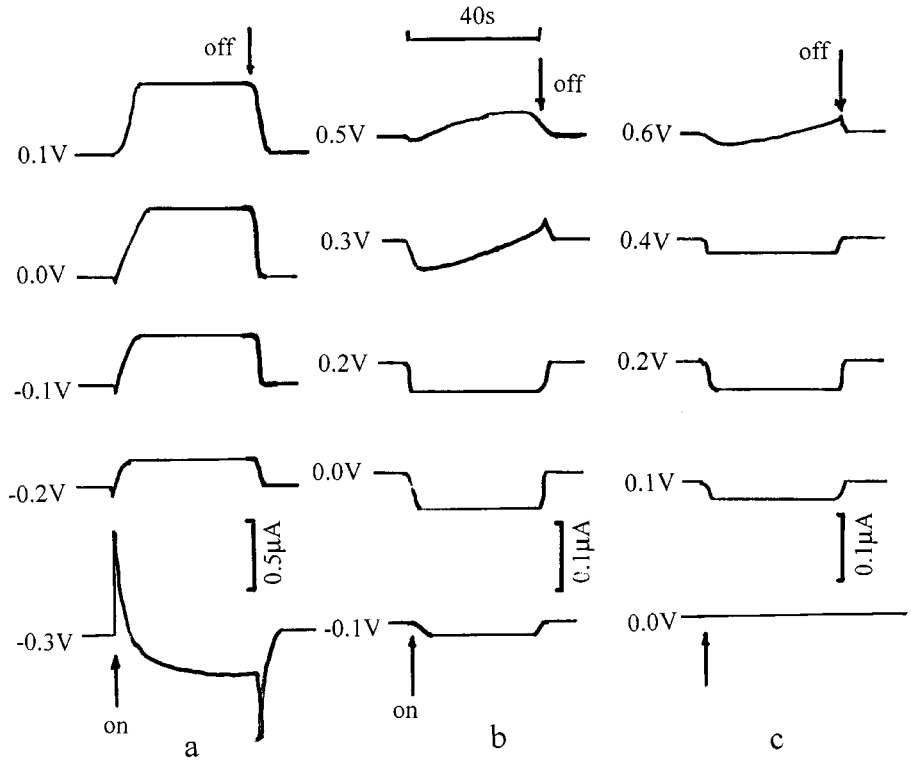

Figure 11 The transient photocurrents at different electrode potentials for samples prepared at pH 3.6 (a) 0.5%; (b) 5%; and (c) 10% Fe. White light was used as incident light.

a converse result was obtained at the electrode potential range from −0.2–0 V, i.e., a cathodic photocurrent appeared only at the beginning of switching on the light, then with the prolongation of illumination time the photoresponse converted to steady anodic photocurrent; then the n-type photoresponse appeared at the electrode potential of 0.1 V. When Fe(III) content was 5%, an obvious transition from p-type photoresponse (cathodic photocurrent) to n-type photoresponse (anodic photocurrent) appeared in the electrode potential range of −0.1–+0.3 V, then n-type photoresponse appeared at electrode potential of +0.5 V which was substantially in agreement with Bard's result [21]. In Bard's paper, an *i-V* curve of p-Si/n-TiO_2 can be divided into three regions, in one region (negative electrode potential) cathodic photocurrent appeared, in another region there was no photoresponse, while in the third region (positive electrode potential) anodic photocurrent was obtained. When Fe content was 10%, the cathodic photocurrents (p-type photoresponse) appeared in the range of +0.1–+0.6 V and the anodic photocurrents (n-type photoresponse) may appear at more positive potential.

All these results can be explained from the electronic structure and the position of energy state of Fe(III)-doped TiO_2 nanocrystalline electrode. According to the theory of solid chemistry [22], the doping of metal ions with lower valence than Ti(IV) resulted in the formation of p-type semiconductor. So Fe(III)-doped TiO_2 nanoparticles can be considered as a heterogeneous system consisting of a surface solid solution and the matrix (anatase) whose energy states are shown in Fig. 12.

At negative potential, the Fermi level of semiconductor can lower than the potential of counter electrode which is favor of the transfer of hole (h^+_{vb}) through external circuit to the counter electrode and electron (e^-_{cb})

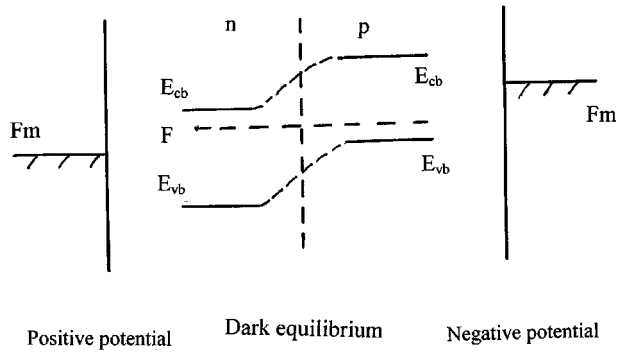

Figure 12 The scheme of relative energy states of p-n junction and electrode potential.

reacted with acceptor at the interface of semiconductor-solution and generated cathodic photocurrent. At positive potential, the Fermi level of semiconductor is higher than the potential of counter electrode which favor of the transfer of electron (e^-_{cb}) through external circuit to counter electrode and hole (h^+_{vb}) reacted with donor at the interface of semiconductor-solution and generated anodic photocurrent. In fact, the two processes both existed and competed each other, one of which was predominant depending on the electrode potential. With the increase of Fe(III) content, more photoexited h^+_{vb} was generated, so the characteristic of p-type became more obvious and the conversion potential became more positive, but the photocurrent became much smaller due to the competition and compensation of anodic and cathodic photocurrents.

4. Conclusion

The nanoparticles of Fe(III)-doped TiO_2 with different Fe(III) content were prepared at different pH using

hydrothermal method and appeared several differences in the structure and morphologies.

1. At pH 1.8, anatase, brookite and trace of hematite coexisted even the Fe(III) content was as low as 0.5% and iron distributed non-uniformly between particles. Although iron can't be detected in smaller particles it is still possible that the solid solution of iron-titanium oxides formed beside the existence of α-Fe_2O_3.

2. At pH 3.6, the phases of products are similar as the above, i.e., anatase, brookite and hematite coexisted but the distribution of iron was a little different from the above. In the samples prepared at pH 1.8, iron can't be detected in smaller particles, while in the samples prepared at pH 3.6, a plenty of iron was detected, indicating that the distribution of Fe(III) ions is more uniform in samples prepared at pH 3.6 than that in the samples prepared at pH 1.8.

3. At pH 6.0, the results showed only anatase existed when Fe(III) content was $\leq$20% and uniform solid solution of iron-titanium oxides formed.

The measurement of photocurrent at different electrode potentials showed the phenomena of p-n photoresponse coexistence. The higher the Fe(III) content, the smaller was the photocurrent, and the more positive was the conversion potential for samples prepared at same pH. On the other hand, the higher the pH, the larger was the photocurrent and the more positive was conversion potential for samples containing the same amount of Fe(III).

Fe(III)-doped TiO_2 samples with different structure can be prepared under different conditions and could be used in different applications, such as photocatalysts or photoanodes in the study of photoelectrochemical solar cells.

Acknowledgement

The authors thank Doc. Peng Jiang of Department of Chemistry, Peking University, for help in doing the AFM. Support from the National Natural Science Foundation of China (Project number 29673003) and Doctoral Program Foundation of Higher Education is gratefully acknowledged.

References

1. B. O. REGAN and M. GRÄTZEL, *Nature* **353** (1991) 737.
2. U. JORSKTEN, J. MOSERr and M. GRÄTZEL, *Chem. Mater*. **6** (1994) 858.
3. J. A. NAVIO *et al., J. Mater. Sci*. **27** (1992) 3036–3042.
4. M. I. LITTER and J. A. NAVIO, *J. Photochem. Photobiol. A Chem*. **98** (1994) 183.
5. *Idem., J. Mol. Catal*. **106** (1996) 267.
6. R. I. BICKLEY and J. S. LEESESAL, *J. Chem. Soc. Faraday Trans*. **88** (1992) 377.
7. R. I. BICKLEY, T. GONZALEZ-CARRENO *et al., ibid.* **90** (1994) 2257–2264.
8. D. CORDISHI, N. BURRIESCI *et al., J. Solid State Chem*., **56** (1985) 182.
9. R. I. BICKLEY *et al*., "Preparation of Catalasts IV" (Elsevier, Amsterdam, 1987) p. 297.
10. M. I. LITTER and J. A. NAVIO, *J. Photochem. Photobiol. A: Chem*. **98** (1996) 171–181.
11. M. R. HOFFMANN, S. T. TARTIN, WONG CHOI and D. W. BAHNEMANN, *Chem. Review* **95** (1995) 69.
12. M. SCHIVELLO, L. RIZZUTI, R. I. BICKLEY *et al.*, in Proceedings of the International Congress on Catalysis (Verlag Chemie, Basel, Berlin, 1980) Vol. III, p. 383.
13. J. C. CONESA, J. SORIA, V. AUGUGLIARO *et al*., in "Structure and Reactivity of Surfaces" (Elsevier, Amsterdam, 1989) p. 30.
14. G. N. SCHRAUZER and T. D. GUTH, *J. Amer. Chem. Soc*. **99** (1977) 7189.
15. V. AUGUGLIARO, A. LAURUCELLA, L. RIZZUTI *et al*., Int. *J. Hydrogen Energy* **79** (1982) 845.
16. V. AUGUGLIARO, F. DALSA, L. RIZZUTI *et al., ibid.* **7** (1982) 851.
17. M. V. TSODIKOV and O. V. BUCHTENKO *et al., J. Mater. Sci*. **30** (1995) 1087.
18. HUMIN CHENG and JIMING MA *et al*., *Chem. Mater*. **7** (1995) 663–671.
19. *Idem. et al*., *Chem. J. Chinese Universities* **11** (1996) 833–837.
20. WONGYONG CHOI, A. TERMIN and M. R. HOFFMANN, *J. Phys. Chem*. **98** (1994) 13669.
21. PAUL A. KOHL, STEVEN N. FRANK and ALLEN J. BARD, *J. Electrochem. Soc.* **124** (1977) 226.
22. MIEZENG SU, "Introduction of Solid Chemistry" (Peking University, 1987) pp. 106–134.

Received 19 January
and accepted 15 December 1998